

GoDe: Gaussians on Demand for Progressive Level of Detail and Scalable Compression

Francesco Di Sario
University of Turin, Italy
francesco.disario@unito.it

Riccardo Renzulli
University of Turin, Italy
riccardo.renzulli@unito.it

Marco Grangetto
University of Turin, Italy
marco.grangetto@unito.it

Akihiro Sugimoto
National Institute of Informatics, Japan
sugimoto@nii.ac.jp

Enzo Tartaglione
LTCI, Télécom Paris, Institut Polytechnique de Paris, France
enzo.tartaglione@telecom-paris.fr

Abstract

3D Gaussian Splatting enhances real-time performance in novel view synthesis by representing scenes with mixtures of Gaussians and utilizing differentiable rasterization. However, the high storage and VRAM requirements of 3DGS limit its deployment in resource-constrained environments, necessitating effective pruning and compression strategies to enable broader applicability. While existing methods are effective in certain scenarios, they lack scalability and adaptability to varying computational constraints, such as hardware capabilities or bandwidth limitations, often necessitating costly model retraining under different configurations. In this work, we introduce a novel and model-agnostic scalable compression framework for 3D Gaussian Splatting models. By leveraging our gradient-informed masking and compression algorithm, we construct a multi-level Gaussian hierarchy that efficiently balances quality and storage efficiency. At inference time, our method enables dynamic scaling across multiple compression levels without retraining, achieving comparable or superior results to state-of-the-art non-scalable compression approaches. We validate our approach on typical datasets and benchmarks, showcasing low distortion and substantial gains in terms of scalability and adaptability. The source code, provided in the supplementary material, will be open-sourced upon acceptance of the paper.

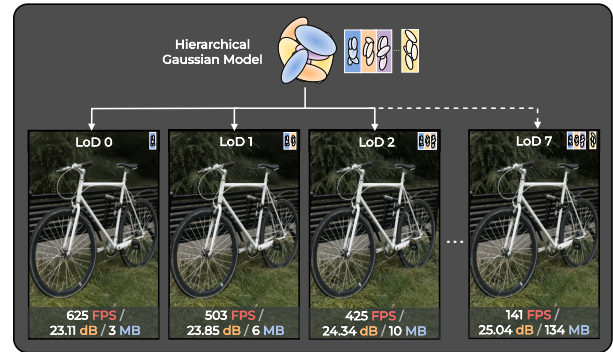


Figure 1. Our method builds a progressive Gaussian hierarchy, enabling adaptive LoD. Combined with compression, it supports multiple rates (eight in the figure), from high to low compression. The model can dynamically adjust based on criteria such as a target minimum FPS.

1. Introduction

Neural Radiance Fields (NeRFs) [26] have consistently boosted novel view synthesis, achieving state-of-the-art quality in scene reconstruction. However, its limitations lie in slow training and inference times. Over the last few years, different methods [6, 13, 14, 17, 29, 36] have been proposed to enhance speed, but none have successfully achieved real-time performance for complex, high-resolution scenes. 3D Gaussian Splatting (3DGS) [18] represents a major advancement by modeling scenes as mixtures of Gaussians, effectively replacing the computationally intensive tasks of ray casting, ray

sampling, and neural network queries. By leveraging differentiable rasterization and spherical harmonics for handling view-dependent effects, 3DGS achieves real-time performance even in complex real-world scenarios and at high-definition resolution.

3DGS offers competitive training times and reconstruction quality that can rival or even surpass that of NeRF-based models. Despite these advancements, some challenges still persist. Specifically, 3DGS models often require large storage and VRAM resources, as scene representations may involve millions of Gaussians. This may hinder real-time rendering on consumer-level devices and make on-demand streaming of 3DGS model quite prohibitive. This has sparked interest in pruning and compression techniques to reduce VRAM consumption during runtime and minimize storage requirements, with high rendering quality. While current pruning and compression methods [2, 3, 12, 15, 31, 40] have shown effectiveness in improving performance and reducing VRAM usage, they lack *scalability*: they require further optimization and personalization for each specific compression level, resulting in multiple models, one for each compression level.

To address this scalability issue, we propose GoDe (**G**aussians **o**n **D**emand), a novel approach that enables scalable compression. As shown in Fig. 1, GoDe enables a 3DGS model to scale across different compression rates, without the need for retraining specialized models. Specifically, GoDe employs a progressive Level of Detail (LoD) approach: Gaussians are organized into discrete and progressive levels, with each level adding more detail (enhancement) to the previous one. This progressive structure allows 3DGS models to be highly scalable across different scenarios. In fact, by adding or removing enhancement layers, we can easily adjust the trade-off between quality and performance. When combined with a compression technique scheme, this approach enables scalable compression. Each level of detail can be seen as a distinct compression level, where higher LoDs corresponds to lower compression rate and lower LoDs corresponds to a higher compression rate. This allows for navigating the rate/distortion curve by simply adding or removing enhancement layers. To build the hierarchy, inspired by iterative gradient-informed pruning approaches, we developed an iterative gradient-informed masking methods that progressively constructs the hierarchy in a top-down manner (from high to low levels). This method is general and compatible with popular 3DGS baselines. A quantization-aware fine-tuning phase ensures coherence and smoothness across the levels, while a final compression step further reduce model size. In summary, our main contributions are:

- **A general method for progressive LoD** (Sec. 3.1):

We propose a novel gradient-based iterative masking technique, which effectively organizes primitives into a hierarchy of progressive levels. Our approach demonstrates high scalability (Sec. 4.4.1) and outperforms other methods in organizing the hierarchy (Sec. 4.4.2).

- **Smooth and continuous transitions between levels** (Sec. 3.2): Our fine-tuning procedure provides an effective method for achieving smoother transitions, significantly enhancing reconstruction quality by finding the optimal balance between different levels of detail. Transitions are further smoothed through a linear opacity interpolation mechanism, minimizing pop-up effects (Sec. 4.3).
- **Scalable Compression** (Sec. 3.3): By incorporating quantization-aware fine-tuning and entropy coding, our method achieves state-of-the-art compression-quality trade-offs (Sec. 4.2), enabling navigation along the rate-distortion curve. This results in a negligible quality loss compared to non-compressed models (Sec. 4.4.3).

We evaluate our method on various 3DGS architectures and compare it against the most recent state-of-the-art methods, showing comparable and even superior performances than non-scalable method. Our method allows models to scale across a wide range of compression levels, from low to very high, achieving up to 99.37% reduction in model size and 98.36% in the number of primitives in the highest compression rate with respect to non-compressed models, while preserving comparable full-size model quality at the lowest compression rate.

2. Background and Related Work

2.1. 3DGS Preliminaries

3DGS [18] has emerged as a cutting-edge technique for real-time radiance field rendering, delivering top-tier performance in both quality and speed. It represents a scene using volumetric Gaussian primitives, each defined by a set of parameters: a position \mathbf{x} , a covariance matrix Σ , which is decomposed into scaling and rotation components, an opacity o , and Spherical Harmonics (SH) coefficients to capture view-dependent color or appearance. In the rendering stage, the 3D primitives are projected into 2D screen space and rasterized with alpha blending $\alpha = oG$ [42] with the projected Gaussian’s contribution to position \mathbf{x} given by $G(\mathbf{x}) = \exp(-\frac{1}{2}(\mathbf{x}^T)\Sigma^{-1}(\mathbf{x}^T))$. The combined effect of converting SHs to per-view color values and applying alpha blending reconstructs the appearance of the captured scene. These primitives originate from a sparse Structure-from-Motion (SfM) point cloud and are optimized through a gradient-descent process, combined with adaptive refinements. This ensures the optimization of both pixel-wise similarity and structural

similarity.

2.2. 3DGS Level of Detail

LoD is a well-established technique in computer graphics, used to optimize performance and improve visual quality. Recent work has extended LoD to 3DGS, primarily to mitigate aliasing artifacts [41] and improve performance, especially for large-scale datasets [24]. These methods typically involve learning multiple levels of detail within the scene representation, followed by selective rendering according to heuristics such as pixel coverage (i.e., the number of pixels occupied by a Gaussian projection on the image plane) and distance from the camera. Other works propose a hierarchical representation, often structured as a tree, as proposed by [19, 34]. This method dynamically implements LoD by selectively rendering Gaussians up to a specific level within the structure based on certain heuristics. Our technique is orthogonal to these works and can be integrated into dynamic LoD systems, where levels serve as an upper bound on active primitives. A related resolution-based LoD method [35] iteratively refines from a minimal representation, but suffers from three key limitations: high iteration count (30k per level), dependence on stored opacity values from previous levels, and rapid Gaussian proliferation at higher levels. In contrast, our approach supports an arbitrary number of levels without additional overhead, requiring only 30k iterations in total while maintaining a compact parameter count. Moreover, it generalizes across models and integrates compression for further efficiency.

2.3. 3DGS Compression

Since the introduction of hybrid radiance fields models that incorporate auxiliary data structures to accelerate training and inference times, such as voxel grids [6, 14, 30, 36], research has focused on compression [9] and complexity reduction [10]. For instance, [9] demonstrates how an iterative-magnitude pruning approach is highly effective in reducing the number of parameters even in the context of radiance fields. These techniques have recently been adapted in the field of 3DGS. In fact, despite its advantages, 3DGS is limited by high storage and memory demands, reducing its application, for example, on low-end hardware. Current compression methods aim at achieving the highest quality at minimal storage size. Typically, compact representations involve post hoc Gaussian pruning followed by compression stages, including quantization (both during and after training) and entropy coding [1, 2, 32, 39]. Some methods operate directly during training, with the aim of limiting the number of Gaussians through learned masks and optimized encoding schemes [7, 15, 23, 33, 37]. Other studies enhance the representation by employing neural networks for on-the-fly Gaussian generation [25],

tri-planes [38], or by using auxiliary structures such as hash grids to store spherical harmonics [7, 22], further reducing storage demands. In particular, Scaffold-GS [25] reduces storage by up to 5 times by replacing Gaussians with anchor points. These anchor points, which are significantly fewer in number, are associated with a set of features, offsets, and scalings. A set of shallow neural networks processes each anchor point and generates the parameters of view-adaptive Gaussians. However, while these methods enable compression, they lack practical scalability. Adjusting compression rates requires either retraining from scratch or additional fine-tuning for each level, limiting their adaptability to scenarios with varying hardware constraints or bandwidth limitations. In contrast, our method incorporates a scalable compression scheme, enabling multiple compression levels from a single training run. This allows instant navigation of the rate-distortion curve without additional optimization. Moreover, our approach achieves performance comparable to, or even exceeding, dedicated non-scalable compression techniques.

3. Gaussians on demand

This section presents our framework for progressive LoD and scalable compression. Our approach extends the standard 3DGS framework by introducing a progressive hierarchy of Gaussians, with varying levels of detail. The objective is to develop a single, scalable model that can dynamically adapt to different compression levels, rendering budgets, and hardware or network constraints. We present a novel algorithm that constructs this hierarchy implicitly, enabling the model to learn multiple levels of detail. We first describe how to build the progressive hierarchy of Gaussians from a pre-trained 3DGS model (Sec.3.1), which forms the basis for constructing adaptable LoDs. Then, we explain how to train and fine-tune Gaussians for each level of detail (Sec. 3.2). Finally, we describe our scalable compression method (Sec. 3.3).

3.1. Hierarchy of Gaussians

Let L denote the total number of levels of detail in the hierarchy. To implement progressive LoD, our objective is to organize the Gaussians of model \mathcal{G} as a sequence of progressive levels $l \in \{0, \dots, L-1\}$ defined as

$$\mathcal{G} = (\mathcal{G}_0, \mathcal{E}_1, \dots, \mathcal{E}_l, \dots, \mathcal{E}_{L-1}), \quad (1)$$

where \mathcal{G}_0 denotes a set of starting Gaussians, and \mathcal{E}_l is the set of enhancement Gaussians at level l . We also refer to \mathcal{G} as \mathcal{G}_{L-1} . The progressive LoD \mathcal{G}_l at a given level l is defined as:

$$\mathcal{G}_l = \mathcal{G}_0 \cup \bigcup_{i=1}^l \mathcal{E}_i. \quad (2)$$

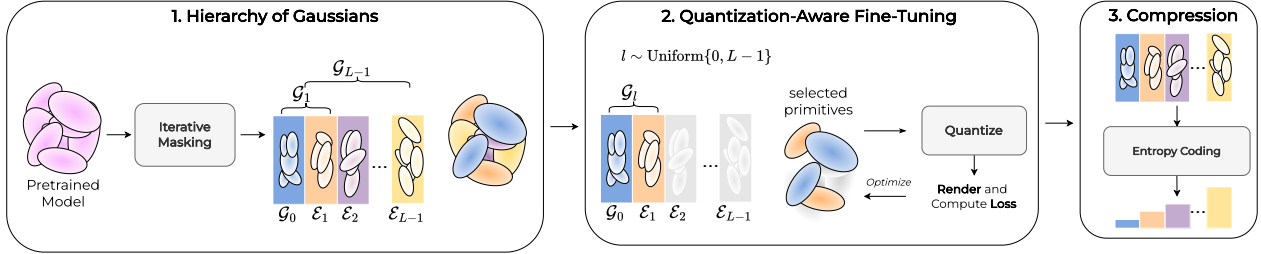


Figure 2. Graphical overview of our method GoDe. 1) Starting from a pre-trained model, we build a progressive hierarchy of Gaussians through iterative gradient-informed masking. 2) A quantization-aware fine tuning stage enhances the model’s quality and reduces its memory footprint. 3) The model is further compressed through entropy coding.

The sets are organized progressively, ensuring that

$$\mathcal{G}_0 \cap \mathcal{E}_1, \dots, \cap \mathcal{E}_l, \dots, \cap \mathcal{E}_{L-1} = \emptyset. \quad (3)$$

This guarantees that each level of detail progressively introduces new Gaussians, with no overlap among the layers. In order to define how many Gaussians are associated with each enhancement set, we define the number of Gaussians $|\mathcal{G}_l|$ associated with level of detail l as:

$$|\mathcal{G}_l| = c_{\min} \cdot b^l, \quad (4)$$

where b is computed as

$$b = \exp\left(\frac{\log(|\mathcal{G}_{L-1}|) - \log(c_{\min})}{L-1}\right) \quad (5)$$

and $c_{\min} = |\mathcal{G}_0|$ is the number of Gaussians at the first LoD level (chosen as desired). We choose this progression since the rate-distortion functions generally follow a logarithmic law (see the theoretical rate-distortion curve for a Gaussian source [8]). This logarithmic progression is chosen to reflect the diminishing returns of adding additional Gaussians, but alternative progression schemes could be employed based on specific application constraints (e.g., computational capabilities of the rendering devices). To organize the Gaussians of the model into a hierarchical structure, we employ an iterative gradient-informed masking process. This approach follows a top-down strategy, starting with the construction of the higher enhancement levels first, namely, progressively building the model’s hierarchy from layer $l = L - 1$ to layer $l = 1$. The base layer \mathcal{G}_0 will consist of the remaining Gaussians at the end of the process. The gradient of each Gaussian parameter serves as a critical indicator of its relevance to the overall model. A Gaussian with a low gradient indicates minimal contribution to the loss function. Conversely, a high gradient suggests that the Gaussian is essential and has a significant impact on the loss. We leverage this gradient information to construct the hierarchy. Specifically, to create the enhancement set \mathcal{E}_l , we accumulate gradients on

\mathcal{G}_l using the training set in order to select the k_l Gaussians with the lowest importance score defined as the sum of the norm of the gradient of all parameters of each Gaussian:

$$\mathcal{E}_l = \text{lowest}_{k_l} \left\{ \left\| \frac{\partial \mathcal{L}}{\partial \theta_i} \right\|_2 \right\}_{i \in \mathcal{G}_l}, \quad (6)$$

where lowest_{k_l} selects the set of the k_l Gaussians with the lowest gradient norm. Note that the difference $|\mathcal{G}_l| - |\mathcal{G}_{l-1}|$ is our k_l . The selected Gaussians are associated with \mathcal{E}_l and masked from further consideration in the next iterations. We reset the gradients and repeat the process. Although this phase requires $L - 1$ steps, it tends to be very fast (1-2 minutes in total to build the hierarchy) as it only requires a single pass through the training set per step. By the end of this process, important Gaussians (those with high gradients) are positioned at lower levels, contributing to coarse details, while less important Gaussians are placed at higher levels, modeling finer geometries and details.

3.2. Quantization-Aware Fine-tuning

This phase involves F fine-tuning iterations. A random level l is uniformly sampled at each iteration and a fine-tuning iteration is performed only on the \mathcal{G}_l Gaussians associated with the selected level l . This optimization enhances reconstruction quality, particularly at the lower levels, while also ensuring smoother transitions between them. During fine-tuning, we integrate quantization-aware training by quantizing spherical harmonic coefficients, opacity, scaling, and rotation parameters. Quantization is applied before the forward pass. To enable gradient flow through quantized parameters, a straight-through estimator is used, which allows backpropagation to proceed as if quantization were absent. More details are given in the Supplementary Sec. 7. Since spherical harmonic coefficients are the most storage-intensive parameters, we further apply a L1 loss to encourage sparsity. Specifically, given the set of spherical harmonics coefficients \mathcal{C}_l associated with the Gaussians in level \mathcal{G}_l we introduce the

penalty term:

$$\mathcal{L}_{SH} = \lambda \sum_i \|\mathbf{C}_{l,i}\|_1. \quad (7)$$

3.3. Scalable Compression and Adaptive Rendering

After fine-tuning, a further compression step is applied. Compression is performed on the first LoD \mathcal{G}_0 as well as on the subsequent enhancement levels \mathcal{E}_l . This inherently enables scalable compression, where each level of detail can be interpreted as a compression stage. Specifically, lower LoDs correspond to higher compression rates, whereas higher LoDs yield lower compression. Each level can be progressively decoded starting from the previous one. Thus, the rate-distortion trade-off can be controlled simply by concatenating enhancement layers. As demonstrated in Sec. 4, our approach achieves highly competitive results compared to the state-of-the-art, with the added benefit of relying on a single scalable model derived from a unified training process. This hierarchical organization can also be leveraged for adaptive rendering at varying levels of detail. More specifically, enhancement layers can be progressively splatted until a target criterion, such as a minimum frame rendering time threshold, is met. To prevent pop-up artifacts and ensure smooth transitions between LoDs, we introduce continuous transitions by linearly interpolating the opacity values of Gaussians in the subsequent enhancement layer. We define a vector of N increasing interpolation factors:

$$\mathbf{t} = \{t_1, t_2, \dots, t_N\}, \quad t_i \in [0, 1], \quad t_1 < t_2 < \dots < t_N \quad (8)$$

and scale the Gaussians’ opacities in the enhancement layer accordingly. In conclusion, GoDe enables 3D Gaussian Splatting models to achieve scalable compression and adaptive rendering, providing state-of-the-art rate-distortion trade-offs.

4. Experiments

4.1. Setup

The code was developed in Python 3.9 using PyTorch 2.1 and executed on a single NVIDIA A40 GPU. We set $L = 8$ for all the configurations, $c_{\min} = 100,000$ and $\lambda = 10^{-2}$. The fine-tuning phase comprises $F = 30,000$ iterations. All the other parameters remain unchanged from the original implementation. Our method was evaluated with four popular 3D Gaussian Splatting models: 3DGS [18], MCMC-3DGS [20], a variant of 3DGS that treats 3D Gaussians as samples from a Markov Chain Monte Carlo process, generally yielding slightly better results than 3DGS, the neural-based Scaffold-GS [25] and the neural and dynamic-LoD-based Octree-GS [34]. The spherical harmonic coefficients are quantized to 8-bit integers, while opacity, scaling, and rotation parameters are quantized to 16-bit floating-point values. Position

parameters remain unquantized. For Scaffold-GS and Octree-GS the implementation is similar to the explicit models. Specifically, we quantize the anchor point features to 8-bit integers, while all the other parameters are quantized to 16-bit floating point values. To build the hierarchy, we use the gradient accumulated at each anchor point, constructing a progressive hierarchy of anchor points. After fine-tuning the model parameters are compressed using the LZMA algorithm.

4.2. Quantitative Results

We evaluated our method on the same datasets used by 3DGS, namely: Mip-NeRF360 [4], TanksAndTemples [21], and DeepBlending [16]. For each test, we report image quality metrics (PSNR, SSIM, LPIPS, computed on VGG), the model size in megabytes (SIZE), the number of primitives $|\mathcal{G}_{L-1}|$ (here W for brevity), and the average frame rate on the test set (FPS). We present the results for each architecture, comparing them with various state-of-the-art proposals. To ensure a fair comparison, all the methods were re-trained and evaluated on our machine, for known discrepancies in reported results as noted by [5]. Additionally, some methods were re-trained using updated hyperparameters to generate rate-distortion curves in alignment with the parameters specified in their respective papers. The main results are summarized in Tab. 1. In Fig. 3, we plot rate-distortion and PSNR/FPS curves. These findings show that our method is generally competitive with current state-of-the-art approaches while benefiting from being a scalable model, as our rate/distortion curve is generated instantly. We divide our analysis of the results between neural-based 3DGS models and explicit ones, as the former generally provides superior rate-distortion performance. Notably, the models obtained with our method are highly scalable, ranging from an extremely high compression rate of a few megabytes to an extremely low one.

Neural-based 3DGS To the best of our knowledge, HAC [7] represents the current state-of-the-art in terms of rate distortion. HAC uses the Scaffold-GS [25] codebase. Scaffold-GS provides slightly higher reconstruction quality than 3DGS (approximately +0.3 dB) while reducing storage by about $5\times$. By applying our method to Scaffold-GS and Octree-GS we observe that it delivers comparable results, slightly outperforming HAC on the Mip-NeRF360 and Tanks&Temples datasets, while HAC remains slightly superior only on the DeepBlending dataset. We consider our results competitive, as our scalable compression method does not require re-training, unlike other methods that need to train a separate model with different hyperparameters. Our method offers another advantage beyond scalability: by masking a higher number of anchor points on average,

Table 1. Comparison of our methods against recent methods. All methods have been retrained and tested on the same hardware. For clarity, we present three compression levels out of 8 for our configurations, selected to match the compression rate of the other methods. These levels, labeled as *Ours*, are derived from the same model without the need for retraining. Red and yellow respectively indicates the first and the second best result.

Method	Mip-NeRF360						Tanks&Temples						Deep Blending					
	PSNR↑	SSIM↑	LPIPS↓	Size[MB]↓	W↓	FPS↑	PSNR↑	SSIM↑	LPIPS↓	Size[MB]↓	W↓	FPS↑	PSNR↑	SSIM↑	LPIPS↓	Size[MB]↓	W↓	FPS↑
Ours	27.43	0.811	0.271	49.0	1546	197	23.75	0.84	0.230	26.6	935	230	29.77	0.905	0.325	28.9	962	327
3DGS	27.30	0.804	0.293	20.6	603	282	23.65	0.834	0.244	13.6	437	337	29.78	0.904	0.333	14.8	451	465
	26.63	0.776	0.341	8.6	242	391	23.12	0.813	0.278	7.0	208	470	29.70	0.900	0.348	7.4	212	622
Ours	27.55	0.817	0.261	47.3	1546	143	24.04	0.845	0.217	26.6	938	178	29.73	0.903	0.326	26.7	965	267
3DGS-MCMC	27.37	0.806	0.288	19.9	603	214	23.85	0.836	0.238	13.3	438	246	29.70	0.902	0.335	13.6	452	356
	26.75	0.775	0.338	8.4	242	299	23.22	0.812	0.278	6.8	208	359	29.59	0.898	0.350	7.0	212	459
Ours	27.77	0.810	0.284	19.6	248	84	24.01	0.848	0.224	11.0	141	116	30.26	0.906	0.339	6.2	80	168
Scaffold-GS	27.61	0.803	0.297	14.1	179	94	23.96	0.844	0.231	8.9	128	128	30.02	0.901	0.350	4.5	58	180
	27.24	0.789	0.318	10.2	129	108	23.86	0.839	0.242	7.3	93	134	29.76	0.897	0.359	3.9	50	184
Ours	27.73	0.813	0.271	19.5	262	71	24.40	0.856	0.242	13.2	173	65	30.10	0.902	0.338	7.3	103	135
Octree-GS	27.49	0.802	0.291	13.9	186	81	24.25	0.847	0.262	9.7	127	72	29.98	0.900	0.348	4.5	64	146
	27.01	0.780	0.322	10.0	133	92	24.01	0.834	0.286	7.1	93	78	29.87	0.898	0.352	4.0	56	146
HAC (low) [7]	27.78	0.812	0.277	22.0	501	68	24.37	0.853	0.215	11.1	307	88	30.34	0.909	0.329	6.3	196	166
HAC (high) [7]	27.17	0.798	0.306	11.5	371	74	24.03	0.843	0.237	7.4	261	82	29.92	0.903	0.350	3.9	180	166
RDO [37]	27.05	0.801	0.288	23.3	1860	178	23.32	0.839	0.232	11.9	912	257	29.72	0.906	0.318	18.0	1478	200
Reduced-3DGS [33]	27.19	0.810	0.267	29.3	1436	234	23.55	0.843	0.223	14.0	656	358	29.70	0.907	0.315	18.3	990	304
Comp-GS [23]	27.28	0.802	0.283	16.4	485	165	23.62	0.837	0.248	9.8	241	286	29.89	0.904	0.336	10.0	246	254
SOG [28]	27.08	0.799	0.277	40.3	2176	132	23.56	0.837	0.221	22.8	1242	227	29.26	0.894	0.336	17.7	890	236
EAGLES [15]	27.13	0.809	0.278	57.1	1290	156	23.20	0.837	0.241	28.9	651	227	29.75	0.910	0.318	52.4	1192	144
LightGaussian [11]	27.24	0.810	0.273	51.0	2197	161	23.55	0.839	0.235	28.5	1211	225	29.41	0.904	0.329	43.2	956	348
Compact-3DGS [22]	27.02	0.800	0.287	29.1	1429	108	23.41	0.836	0.238	20.9	842	147	29.76	0.905	0.324	23.8	1053	144

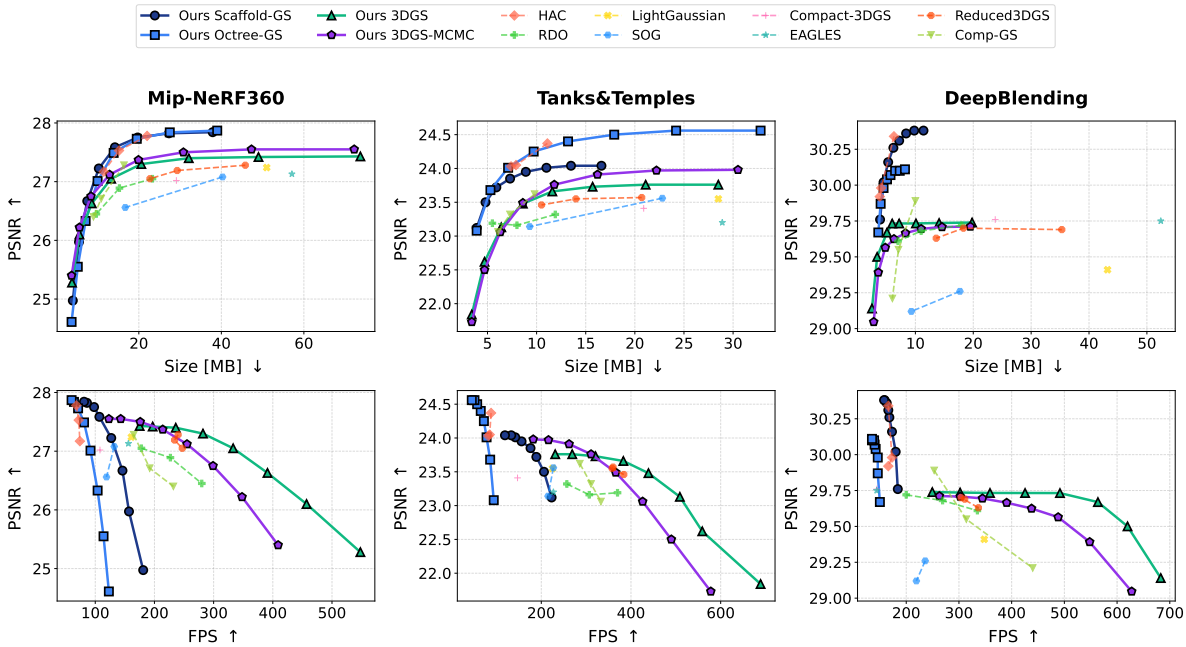


Figure 3. Rate/distortion (above) and PSNR/FPS (below) curves on the three main datasets. Our approach achieves competitive results with both neural-based Gaussian models and explicit ones while maintaining significantly higher speed at comparable quality. It is also the only method that achieves scalability without requiring ad-hoc training.

our model is faster, achieving a frame rate increase ranging from +33% to +62% while maintaining similar reconstruction quality.

Explicit 3DGS Regarding the comparison with explicit Gaussian splatting models, our results are state-of-the-art on nearly every dataset in terms of rate/distortion and performance at equivalent or even superior quality, achieving up to a 3× increase in FPS. There is one point

where Comp-GS [23] slightly outperforms our method, but this approach scales less effectively at higher compression rates. In this case as-well, our approach also offers the advantage of utilizing a single scalable model, which eliminates the need for re-training when adapting to different compression rates.



Figure 4. Visualization of LoDs. For visual purposes, we show the first three LoD levels and the last one. For each LoD we provide the average FPS, PSNR, primitives count W (in thousands), and size. Starting from top to bottom we have: *kitchen*, *counter*, *drjohnson* and *truck* scenes.

4.3. Visualizing LoDs and Transitions

In Fig. 4 we visualize some LoD levels for various scenes. For each LoD level, we report the average frame rate computed for rendering the image of the test set, the number of Gaussians, the average PSNR, and the model size. The transition between LoDs is smooth, due to the fine-tuning process with random LoD sampling. Moreover, we observe that lower LODs are extremely fast and small, with rendering speeds exceeding 900 FPS and model sizes as low as 3.7 MB for the *drjohnson* scene from the DeepBlending dataset (compared to the vanilla-3DGS which renders the same scene at 146FPS and requires 780MB of storage). Similar performance is achieved in other datasets. It is important to note that lower LoDs tend to lose fine details, particularly in high-frequency areas such as reflections, transparency handling, and background elements. This is particularly noticeable in the *kitchen* scene, where at lower levels of detail the glass bottle in the background is either not rendered at all or only partially and becomes progressively more defined at higher levels. Another example can be seen in the *counter* scene, with the reflection on the dishes. Other examples are the painting in the *drjohnson* scene and the trees in the background of

the *truck* scene. This is a significant result, demonstrating the effectiveness of the method, which automatically learns a hierarchy and preserves the most important details at each level, minimizing the loss of detail to secondary aspects. In Fig. 5, we illustrate a seamless transition between two adjacent levels of detail, achieved by linearly interpolating the opacity values of the nearest enhancement layer Gaussians. This approach further minimizes pop-up artifacts. Additional visualizations, including videos, are provided in the supplementary material.

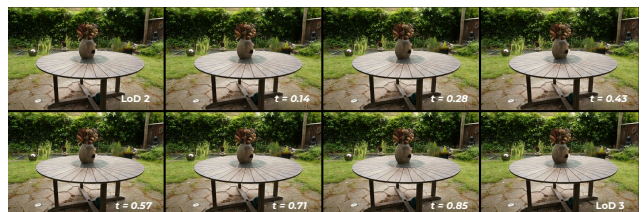


Figure 5. Continuous transitions between two adjacent levels, with eight linear interpolating factors on *Garden* scene.

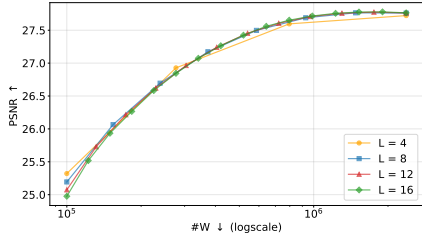


Figure 6. Ablation on the number of levels on Mip-NeRF360.

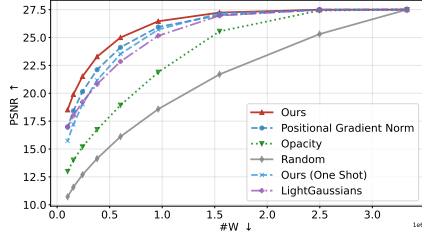


Figure 7. Comparison among pruning methods on Mip-NeRF 360.

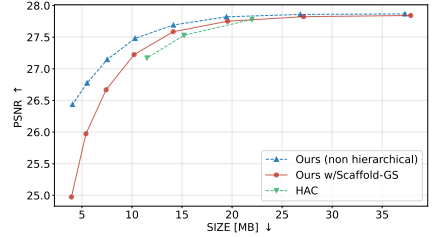


Figure 8. Comparison among our method with Scaffold-GS, a non-scalable variant of the same method and HAC.

4.4. Ablations

Here, we investigate how different choices of parameters and algorithms affect the render quality. These choices include the number of levels L , the ranking methods used to build the masks, the impact of compression, and the hierarchy on quality.

4.4.1. Number of levels

In our configuration, we opted for $L = 8$ levels. However, we tested our method with a variable number of levels and observed minimal differences in performance. Fig. 6 shows that, with increasing number of levels, there is a slight decrease in the quality of lower LoDs, while the quality in higher levels remains similar. We chose 8 levels as a good balance, but our method is easily extendable to a higher number of levels without significant loss in quality. This highlights the scalability of our approach.

4.4.2. Pruning methods

In Fig. 7, we investigate multiple strategies for ranking Gaussians, which are commonly used to prune and compact the model. We found that our method provides better reconstruction quality with the same number of Gaussians compared to several proposed strategies, such as those based on opacity [18] or positional gradient [2]. Additionally, we compared our technique with the one proposed by LightGaussian [11] and still achieved superior results. All these methods have been tested using the same iterative process. We also evaluated the necessity of iterative masking versus the same ranking method but applied in a one-shot manner labeled as *Ours (One Shot)*, where the gradient is accumulated only once to create the levels. Our experiments demonstrate the importance of the iterative approach, as the one-shot method leads to a loss in quality, particularly at lower LoDs. Since the iterative masking process is very fast, we opted to use the sum of the gradient norms of the parameters as a score and perform the masking iteratively.

Table 2. Effects of fine-tuning and compression on Mip-NeRF360.

LoD	W	Mask Only			Fine Tuning			Fine-Tuning + Compression		
		PSNR↑	SSIM↑	Size[MB]↓	PSNR↑	SSIM↑	Size[MB]↓	PSNR↑	SSIM↑	Size[MB]↓
0	100	18.52	0.553	24.1	25.20	0.719	24.1	25.28	0.719	3.8
1	155	19.90	0.606	36.7	26.06	0.752	36.7	26.10	0.751	5.6
2	242	21.52	0.662	56.4	26.65	0.778	56.4	26.63	0.776	8.6
3	381	23.28	0.715	89.1	26.84	0.787	89.1	27.05	0.793	13.3
4	603	25.00	0.760	142.8	27.08	0.796	142.8	27.30	0.804	20.6
5	962	26.45	0.793	216.6	27.33	0.807	69.8	27.40	0.809	32.1
6	1546	27.23	0.810	365.9	27.45	0.813	227.2	27.43	0.811	49.0
7	2497	27.49	0.815	562.2	27.47	0.814	365.6	27.42	0.811	73.7



Figure 9. Effects of fine-tuning on the train scene of *Tanks&Temples* dataset. In the first row, LoDs without fine-tuning; on the second, LoDs after fine-tuning.

4.4.3. Effects of Fine-Tuning and Compression

We analyze the effects of fine-tuning and compression from both a quantitative and qualitative perspective. As shown in Tab. 2, the fine-tuning phase significantly improves reconstruction quality, particularly for lower LoDs, while slightly reducing quality in the two highest LoDs, of about 0.02 dB. Regarding compression, we observe a reduction in storage ranging from 99.37% to 86.88%, depending on the level considered. The impact on reconstruction quality is negligible, with a loss of 0.05 dB in the highest LoD. In Fig. 9, we also visualize the visual impact of fine-tuning. Non-fine-tuned models exhibit holes and generally lower quality, while the LoDs after fine-tuning show improved quality with way fewer artifacts.

4.4.4. Impact of hierarchical representation

In this ablation study, we evaluate our hierarchical compression method against a non-hierarchical variant to assess how much our hierarchical approach diverges from the best achievable performance. Specifically, we re-run our method but omit any hierarchy constraints. The process

is as follows: we accumulate gradients for one epoch, mask the k Gaussians with the lowest gradient values, perform a fine-tuning cycle of 7,000 iterations, and evaluate the performance (each evaluation is a point in Fig. 8). This procedure is repeated across 8 levels, down to a minimum threshold of 50,000 parameters, with each level acting as an independent model. Interestingly, our method sets a new performance benchmark, outperforming HAC and underline the effectiveness of iterative, gradient-based pruning for this task. Our hierarchical version, though also superior to HAC, performs less well, particularly at high compression levels. This is due to the imposed hierarchy, which requires optimizing each level in relation to the others, thus introducing a trade-off between higher and lower levels.

5. Conclusion

This paper presented GoDe, a framework for a progressive level of detail and scalable compression. Our extensive experiments show that our method is highly scalable and competitive, often surpassing non-scalable state-of-the-art techniques in both quality and performance. In fact, unlike previously proposed methods, our approach allows for model compression at multiple rates without the need for retraining with different hyperparameters. This framework also enables adaptive rendering: given the hierarchical-layered structure of the model, it is possible to dynamically select Gaussians up to a certain level to meet specific criteria, such as a target frame rate. Additionally, a notable advantage of our approach is its generality: relying on widely applicable techniques, such as gradient-informed pruning and quantization-aware training, our method can be integrated into popular 3DGS models.

References

- [1] Muhammad Salman Ali, Sung-Ho Bae, and Enzo Tartaglione. Elms: Enhancing memory and computation scalability through compression for 3d gaussian splatting. *arXiv preprint arXiv:2410.23213*, 2024. 3
- [2] Muhammad Salman Ali, Maryam Qamar, Sung-Ho Bae, and Enzo Tartaglione. Trimming the fat: Efficient compression of 3d gaussian splats through pruning. *arXiv preprint arXiv:2406.18214*, 2024. 2, 3, 8
- [3] Milena T. Bagdasarian, Paul Knoll, Yi-Hsin Li, Florian Barthel, Anna Hilsmann, Peter Eisert, and Wieland Morgenstern. 3dgs.zip: A survey on 3d gaussian splatting compression methods, 2024. 2
- [4] Jonathan T Barron, Ben Mildenhall, Dor Verbin, Pratul P Srinivasan, and Peter Hedman. Mip-nerf 360: Unbounded anti-aliased neural radiance fields. In *Proceedings of the IEEE/CVF Conference on Computer Vision and Pattern Recognition*, pages 5470–5479, 2022. 5
- [5] Samuel Rota Bulò, Lorenzo Porzi, and Peter Kotschieder. Revising densification in gaussian splatting. *arXiv preprint arXiv:2404.06109*, 2024. 5, 2
- [6] Anpei Chen, Zexiang Xu, Andreas Geiger, Jingyi Yu, and Hao Su. Tensorf: Tensorial radiance fields. *ECCV*, 2022. 1, 3
- [7] Yihang Chen, Qianyi Wu, Weiyao Lin, Mehrtash Harandi, and Jianfei Cai. Hac: Hash-grid assisted context for 3d gaussian splatting compression. In *European Conference on Computer Vision*, 2024. 3, 5, 6, 2, 4
- [8] T.M. Cover and J.A. Thomas. *Elements of Information Theory*. Wiley, 2012. 4
- [9] Chenxi Lola Deng and Enzo Tartaglione. Compressing explicit voxel grid representations: fast nerfs become also small. In *Proceedings of the IEEE/CVF Winter Conference on Applications of Computer Vision*, pages 1236–1245, 2023. 3
- [10] Francesco Di Sario, Riccardo Renzulli, Enzo Tartaglione, and Marco Grangetto. Boost your nerf: A model-agnostic mixture of experts framework for high quality and efficient rendering. In Aleš Leonardis, Elisa Ricci, Stefan Roth, Olga Russakovsky, Torsten Sattler, and Gül Varol, editors, *Computer Vision – ECCV 2024*, pages 176–192, Cham, 2025. Springer Nature Switzerland. 3
- [11] Zhiwen Fan, Kevin Wang, Kairun Wen, Zehao Zhu, Dejie Xu, and Zhangyang Wang. Lightgaussian: Unbounded 3d gaussian compression with 15x reduction and 200+ fps. *arXiv preprint arXiv:2311.17245*, 2023. 6, 8, 2, 5
- [12] Guangchi Fang and Bing Wang. Mini-splatting: Representing scenes with a constrained number of gaussians. In Aleš Leonardis, Elisa Ricci, Stefan Roth, Olga Russakovsky, Torsten Sattler, and Gül Varol, editors, *Computer Vision – ECCV 2024*, pages 165–181, Cham, 2024. Springer Nature Switzerland. 2
- [13] Sara Fridovich-Keil, Giacomo Meanti, Frederik Rahbæk Warburg, Benjamin Recht, and Angjoo Kanazawa. K-planes: Explicit radiance fields in space, time, and appearance. In *2023 IEEE/CVF Conference on Computer Vision and Pattern Recognition (CVPR)*, pages 12479–12488, 2023. 1
- [14] Sara Fridovich-Keil, Alex Yu, Matthew Tancik, Qinhong Chen, Benjamin Recht, and Angjoo Kanazawa. Plenoxels: Radiance fields without neural networks. In *Proceedings of the IEEE/CVF Conference on Computer Vision and Pattern Recognition*, pages 5501–5510, 2022. 1, 3
- [15] Sharath Girish, Kamal Gupta, and Abhinav Shrivastava. Eagles: Efficient accelerated 3d gaussians with lightweight encodings, 2024. 2, 3, 6, 5
- [16] Peter Hedman, Julien Philip, True Price, Jan-Michael Frahm, George Drettakis, and Gabriel Brostow. Deep blending for free-viewpoint image-based rendering. 37(6):257:1–257:15, 2018. 5
- [17] Wenbo Hu, Yuling Wang, Lin Ma, Bangbang Yang, Lin Gao, Xiao Liu, and Yuewen Ma. Tri-miprf: Tri-mip representation for efficient anti-aliasing neural radiance fields. In *Proceedings of the IEEE/CVF International Conference on Computer Vision*, pages 19774–19783, 2023. 1
- [18] Bernhard Kerbl, Georgios Kopanas, Thomas Leimkühler, and George Drettakis. 3d gaussian splatting for real-time radiance field rendering. *ACM Transactions on Graphics*, 42(4), 2023. 1, 2, 5, 8
- [19] Bernhard Kerbl, Andreas Meuleman, Georgios Kopanas, Michael Wimmer, Alexandre Lanvin, and George Drettakis. A hierarchical 3d gaussian representation for real-time rendering of very large datasets. *ACM Transactions on Graphics*, 43(4), July 2024. 3
- [20] Shakiba Kheradmand, Daniel Rebain, Gopal Sharma, Weiwei Sun, Jeff Tseng, Hossam Isack, Abhishek Kar, Andrea Tagliasacchi, and Kwang Moo Yi. 3d gaussian splatting as markov chain monte carlo. *arXiv preprint arXiv:2404.09591*, 2024. 5
- [21] Arno Knapitsch, Jaesik Park, Qian-Yi Zhou, and Vladlen Koltun. Tanks and temples: Benchmarking large-scale scene reconstruction. *ACM Transactions on Graphics (ToG)*, 36(4):1–13, 2017. 5
- [22] Joo Chan Lee, Daniel Rho, Xiangyu Sun, Jong Hwan Ko, and Eunbyung Park. Compact 3d gaussian representation for radiance field. *arXiv preprint arXiv:2311.13681*, 2023. 3, 6, 2, 5
- [23] Xiangrui Liu, Xinju Wu, Pingping Zhang, Shiqi Wang, Zhu Li, and Sam Kwong. Compgs: Efficient 3d scene representation via compressed gaussian splatting. In *Proceedings of the 32nd ACM International Conference on Multimedia*, pages 2936–2944, 2024. 3, 6, 4, 5
- [24] Yang Liu, Chuanchen Luo, Lue Fan, Naiyan Wang, Junran Peng, and Zhaoxiang Zhang. Citygaussian: Real-time high-quality large-scale scene rendering with gaussians. In Aleš Leonardis, Elisa Ricci, Stefan Roth, Olga Russakovsky, Torsten Sattler, and Gül Varol, editors, *Computer Vision – ECCV 2024*, pages 265–282, Cham, 2025. Springer Nature Switzerland. 3
- [25] Tao Lu, Mulin Yu, Linning Xu, Yuanbo Xiangli, Limin Wang, Dahua Lin, and Bo Dai. Scaffold-gs: Structured 3d gaussians for view-adaptive rendering. In *Proceedings of the IEEE/CVF Conference on Computer Vision and Pattern Recognition (CVPR)*, pages 20654–20664, June 2024. 3, 5
- [26] Ben Mildenhall, Pratul P Srinivasan, Matthew Tancik, Jonathan T Barron, Ravi Ramamoorthi, and Ren Ng. Nerf: Representing scenes as neural radiance fields for view

- synthesis. In *European conference on computer vision*, pages 405–421. Springer, 2020. [1](#)
- [27] Wieland Morgenstern, Florian Barthel, Anna Hilsmann, and Peter Eisert. Compact 3d scene representation via self-organizing gaussian grids. *arXiv preprint arXiv:2312.13299*, 2023. [2](#), [4](#)
- [28] Wieland Morgenstern, Florian Barthel, Anna Hilsmann, and Peter Eisert. Compact 3d scene representation via self-organizing gaussian grids, 2024. [6](#), [5](#)
- [29] Thomas Müller, Alex Evans, Christoph Schied, and Alexander Keller. Instant neural graphics primitives with a multiresolution hash encoding. *ACM Trans. Graph.*, 41(4):102:1–102:15, July 2022. [1](#)
- [30] Thomas Müller, Alex Evans, Christoph Schied, and Alexander Keller. Instant neural graphics primitives with a multiresolution hash encoding. *ACM Transactions on Graphics (ToG)*, 41(4):1–15, 2022. [3](#)
- [31] KL Navaneet, Kossar Pourahmadi Meibodi, Soroush Abbasi Koochpayegani, and Hamed Pirsiavash. Compigs: Smaller and faster gaussian splatting with vector quantization. *ECCV*, 2024. [2](#)
- [32] Simon Niedermayr, Josef Stumpfegger, and Rüdiger Westermann. Compressed 3d gaussian splatting for accelerated novel view synthesis. In *Proceedings of the IEEE/CVF Conference on Computer Vision and Pattern Recognition*, pages 10349–10358, 2024. [3](#)
- [33] Panagiotis Papantonakis, Georgios Kopanas, Bernhard Kerbl, Alexandre Lanvin, and George Drettakis. Reducing the memory footprint of 3d gaussian splatting. *Proceedings of the ACM on Computer Graphics and Interactive Techniques*, 7(1):1–17, 2024. [3](#), [6](#), [2](#), [4](#), [5](#)
- [34] Kerui Ren, Lihan Jiang, Tao Lu, Mulin Yu, Linning Xu, Zhangkai Ni, and Bo Dai. Octree-gs: Towards consistent real-time rendering with lod-structured 3d gaussians. *arXiv preprint arXiv:2403.17898*, 2024. [3](#), [5](#)
- [35] Yuang Shi, Géraldine Morin, Simone Gasparini, and Wei Tsang Ooi. Lapisgs: Layered progressive 3d gaussian splatting for adaptive streaming. *arXiv preprint arXiv:2408.14823*, 2024. [3](#)
- [36] Cheng Sun, Min Sun, and Hwann-Tzong Chen. Direct voxel grid optimization: Super-fast convergence for radiance fields reconstruction. In *Proceedings of the IEEE/CVF Conference on Computer Vision and Pattern Recognition*, pages 5459–5469, 2022. [1](#), [3](#)
- [37] Henan Wang, Hanxin Zhu, Tianyu He, Runsen Feng, Jiajun Deng, Jiang Bian, and Zhibo Chen. End-to-end rate-distortion optimized 3d gaussian representation. *arXiv preprint arXiv:2406.01597*, 2024. [3](#), [6](#), [2](#), [4](#), [5](#)
- [38] Minye Wu and Tinne Tuytelaars. Implicit gaussian splatting with efficient multi-level tri-plane representation, 2024. [3](#)
- [39] Shuzhao Xie, Weixiang Zhang, Chen Tang, Yunpeng Bai, Rongwei Lu, Shijia Ge, and Zhi Wang. Mesongs: Post-training compression of 3d gaussians via efficient attribute transformation. In *European Conference on Computer Vision*. Springer, 2024. [3](#)
- [40] Shuzhao Xie, Weixiang Zhang, Chen Tang, Yunpeng Bai, Rongwei Lu, Shijia Ge, and Zhi Wang. Mesongs: Post-training compression of 3d gaussians via efficient attribute transformation. In Aleš Leonardis, Elisa Ricci, Stefan Roth, Olga Russakovsky, Torsten Sattler, and Gül Varol, editors, *Computer Vision – ECCV 2024*, pages 434–452, Cham, 2025. Springer Nature Switzerland. [2](#)
- [41] Zhiwen Yan, Weng Fei Low, Yu Chen, and Gim Hee Lee. Multi-scale 3d gaussian splatting for anti-aliased rendering. In *Proceedings of the IEEE/CVF Conference on Computer Vision and Pattern Recognition (CVPR)*, pages 20923–20931, June 2024. [3](#)
- [42] M. Zwicker, H. Pfister, J. van Baar, and M. Gross. Ewa volume splatting. In *Proceedings Visualization, 2001. VIS '01.*, pages 29–538, 2001. [2](#)

GoDe: Gaussians on Demand for Progressive Level of Detail and Scalable Compression

Supplementary Material

In Sec. 6 we present the pseudocode for building the hierarchy and the fine-tune process. In Sec. 7 we provide more details about the quantization-aware training. In Sec. 8 we discuss alternative sampling strategy for the fine-tuning phase. In Sec. 9 we provide a comparison of our method with and without compression enabled. In Sec. 10 we present additional results, including a more comprehensive comparison with state-of-the-art methods (Sec. 10.1), a complete visualization of levels across all scenes (Sec. 10.2) and per-scenes results (Sec. 10.3).

6. Pseudocode

Here, we present the code for constructing the hierarchical Gaussian model and the fine-tuning process. Following Eq. 1, a Hierarchical Gaussian model \mathcal{G} is defined as a base layer \mathcal{G}_0 and a list of enhancement layers \mathcal{E}_s . The process begins with the computation of a progression that determines the number of primitives at each level, as described in Alg. 1. Given a minimum number of Gaussians, c_{\min} , which defines the number of gaussians in the base layer, and the maximum number of Gaussians, c_{\max} , which sets the total count, we compute the progression of k_s . In our experiments, we impose a limit on the total number of Gaussians, capping it at 0.75% of the original model’s count. This progression is chosen based on the observation that rate-distortion curves typically follow a logarithmic pattern. However, it is important to note that our algorithm is independent of this assumption. We then proceed with constructing the hierarchy in a top-down manner, as outlined in Alg. 2, followed by the final fine-tuning step, which is described in Alg. 3.

Algorithm 1 Compute k_s

Input: number of starting Gaussians c_{\min} , maximum number of Gaussians c_{\max} , number of levels L

Output: list of Gaussian counts per level k_s

```
1:  $b \leftarrow \exp\left(\frac{\log(c_{\max}) - \log(c_{\min})}{L-1}\right)$ 
2:  $arr \leftarrow [0, 1, \dots, L-1]$ 
3:  $progr \leftarrow \text{floor}((b^{arr}) \times c_{\min})$ 
4:  $k_s \leftarrow [c_{\min}]$ 
5: for  $i \leftarrow 1$  to  $L-1$  do
6:    $\text{append}(k_s, progr[i] - progr[i-1])$ 
7: end for
8: return  $k_s$ 
```

7. Implementation Details on QA Fine-Tuning

To implement quantization, we used PyTorch’s quantization libraries. The Quantization-Aware Training in PyTorch employs symmetric quantization with fixed intervals and is based on FakeQuantization, which emulates quantization without losing the floating-point representation. This technique is general and easily adaptable to all 3DGS models. Specifically, for explicit models (3DGS and 3DGS-MCMC), we quantized the Spherical Harmonics coefficients to 8-bit integers, while the remaining parameters were quantized to 16-bit floating point, leaving the position values unchanged. For Scaffold-GS and Octree-GS models, the features of the anchor points were quantized to 8-bit integers, while all other parameters, including position, were kept in 16-bit floating point. In both cases, an auxiliary L1 loss was used: for explicit models, it was applied to the SH coefficients, and for neural models, it was applied to the anchor point features. During the forward pass, quantization involves rounding and clipping. Given a floating-point value x , the quantized value x_q is computed as:

$$x_q = \text{clip}\left(\text{round}\left(\frac{x}{\text{scale}} + \text{zero_point}\right), q_{\min}, q_{\max}\right)$$

where q_{\min} and q_{\max} are determined by the number of bits used, scale is defined as $\frac{x_{\max} - x_{\min}}{q_{\max} - q_{\min}}$, and zero_point is calculated as $q_{\min} - \left(\frac{x_{\min}}{\text{scale}}\right)$. After quantization, the value is dequantized as:

$$x_{dq} = (\text{scale} \cdot x_q) - \text{zero_point}.$$

During the backward pass, a straight-through estimator is implemented to bypass the rounding operation.

8. Random Sampling vs Weighted Sampling

In this section, we compare the random sampling approach with alternative sampling strategies. During the fine-tuning phase, the levels are sampled uniformly, following $l \sim \text{Uniform}\{0, L-1\}$, where L denotes the number of levels. Additionally, we explored a weighted sampling strategy that assigns higher probabilities to upper levels. While this method improves the quality of the upper levels, it significantly degrades the quality of the lower ones, as shown in Tab. 3. To implement the weighted sampling, we utilize Eq. 5 and transform the progression of k_s into probabilities, normalizing them between 0 and 1. This results in upper levels receiving higher weights, while

Table 3. Comparison among sampling strategies on Mip-NeRF360 and 3DGS.

level	W	Uniform Sampling			Weighted Sampling (G=5)			Weighted Sampling (G=8)			Weighted Sampling (G=10)		
		PSNR \uparrow	SSIM \uparrow	LPIPS \downarrow	PSNR \uparrow	SSIM \uparrow	LPIPS \downarrow	PSNR \uparrow	SSIM \uparrow	LPIPS \downarrow	PSNR \uparrow	SSIM \uparrow	LPIPS \downarrow
LoD 0	100	25.20	0.719	0.408	24.72	0.706	0.417	24.12	0.693	0.426	23.30	0.675	0.436
LoD 1	155	26.06	0.752	0.372	25.70	0.742	0.379	25.26	0.732	0.386	24.70	0.721	0.392
LoD 2	242	26.65	0.778	0.340	26.41	0.771	0.345	26.13	0.764	0.349	25.90	0.760	0.351
LoD 3	381	27.08	0.796	0.312	26.94	0.792	0.315	26.89	0.791	0.315	26.77	0.788	0.316
LoD 4	603	27.33	0.807	0.291	27.37	0.808	0.289	27.35	0.807	0.289	27.34	0.807	0.288
LoD 5	962	27.45	0.813	0.276	27.56	0.815	0.272	27.58	0.815	0.271	27.58	0.815	0.270
LoD 6	1546	27.47	0.814	0.269	27.58	0.816	0.264	27.61	0.817	0.263	27.63	0.817	0.261
LoD 7	2497	27.47	0.815	0.267	27.57	0.816	0.262	27.60	0.817	0.260	27.62	0.817	0.259
AVG	811	26.84	0.787	0.317	26.73	0.783	0.318	26.57	0.779	0.320	26.36	0.775	0.322

Algorithm 2 Iterative Masking

Input: Pre-trained Gaussian Model \mathcal{G}_p , number of levels

L , progression k_s , training set $\mathcal{D}_{\text{train}}$

Output: Hierarchical Gaussian model $(\mathcal{G}_0, \mathcal{E}_s)$

- 1: $\mathcal{E}_s \leftarrow$ empty list of size $L - 1$
 - 2: $\mathcal{G}_{L-1} \leftarrow \mathcal{G}_p$
 - 3: **for** $l \leftarrow L - 1$ to 1 **do**
 - 4: computeGradients($\mathcal{G}_l, \mathcal{D}_{\text{train}}$)
 - 5: $k_l \leftarrow k_s[l]$
 - 6: $\mathcal{E}_l \leftarrow \text{lowest}_{k_l} \left\{ \left\| \frac{\partial \mathcal{L}}{\partial \theta_i} \right\|_2 \right\}_{i \in \mathcal{G}_l}$
 - 7: append($\mathcal{E}_l, \mathcal{E}_s$)
 - 8: $\mathcal{G}_{l-1} \leftarrow \text{maskGaussians}(\mathcal{E}_l, \mathcal{G}_l)$
 - 9: **end for**
 - 10: reverse(\mathcal{E}_s)
 - 11: **return** $(\mathcal{G}_0, \mathcal{E}_s)$
-

Algorithm 3 Fine Tune

Input: Hierarchical Gaussian Model $(\mathcal{G}_0, \mathcal{E}_s)$, training set

$\mathcal{D}_{\text{train}}$, number of iterations F , boolean *compress*

Output: Fine-tuned Hierarchical Model $(\mathcal{G}_0, \mathcal{E}_s)$

- 1: **for** $i \leftarrow 0$ to F **do**
 - 2: Random sample viewpoint v and level $l \in \{0, |\mathcal{E}_s|\}$
 - 3: $\mathcal{G}_l \leftarrow \mathcal{G}_0 \cup \bigcup_{i=1}^l \mathcal{E}_i$
 - 4: render(\mathcal{G}_l, v)
 - 5: compute loss and optimize \mathcal{G}_l
 - 6: **if** *compress* **then**
 - 7: compressModel($\mathcal{G}_0, \mathcal{E}_s$)
 - 8: **end if**
 - 9: **end for**
 - 10: **return** $(\mathcal{G}_0, \mathcal{E}_s)$
-

lower levels are assigned lower weights, making them less probable. The degree of emphasis on upper levels is controlled by the denominator $(L - 1)$ (here redefined as G for clarity). Increasing G accentuates the bias toward upper levels, whereas reducing tends to an uniform sampling scheme. We tested with G up to 10, observing that uniform sampling of levels generally produces better results, establishing it as an optimal trade-off between

higher and lower levels.

9. Compression vs Not Compression

In Tab. 4, 5, 6 we present the results for all 8 levels and models, both with and without compression. The observed quality loss due to compression is negligible compared to the substantial gains in storage efficiency, especially for explicit models. The maximum quality degradation occurs with MCMC-3DGS on the Mip-NeRF360 dataset, amounting to -0.19dB (LoD 8), while on Tanks&Temples, it is even less significant, reaching only -0.12dB (LoD 8). Remarkably, on the DeepBlending dataset, compression results in a general improvement in quality, with gains of up to +0.23dB (LoD 8), with the exception of Octree-GS.

10. Additional Results

10.1. Comparison with SOTA

We provide a more detailed comparison with recent state-of-the-art methods. We evaluated our method against HAC [7], RDO [37], LightGaussian [11], SOG [27], Compact-3DGS [31], Reduced-3DGS [33], EAGLES [15] and Comp-GS [22], all of which represent the latest advancements in the fields, as also highlighted by [3]. All methods were tested on the same hardware setup. We observed that all results reported in the respective papers are reproducible. However, there are some discrepancies in the *LPIPS* values, as these are often computed without normalizing pixel values between $[-1, 1]$ (which tends to yield higher values, as noted by [5]). We also derived rate/distortion curves for some of the methods. We use the hyperparameters reported from the respective paper, defining 3 levels of compression, high, medium and low, as shown in Tab. 7.

Table 4. Compressed vs Not Compressed models on Mip-NeRF360

Method	LoD	W	Compressed				Not Compressed			
			PSNR \uparrow	SSIM \uparrow	LPIPS \downarrow	Size[MB] \downarrow	PSNR \uparrow	SSIM \uparrow	LPIPS \downarrow	Size[MB] \downarrow
Ours 3DGS	LoD 0	100	25.28	0.719	0.407	3.8	25.20	0.719	0.408	23.7
	LoD 1	155	26.10	0.751	0.371	5.6	26.06	0.752	0.372	35.9
	LoD 2	242	26.63	0.776	0.341	8.6	26.65	0.778	0.340	56.3
	LoD 3	381	27.05	0.793	0.314	13.3	27.08	0.796	0.312	89.0
	LoD 4	603	27.30	0.804	0.293	20.6	27.33	0.807	0.291	141.5
	LoD 5	962	27.40	0.809	0.278	32.1	26.84	0.787	0.317	226.5
	LoD 6	1546	27.43	0.811	0.271	49.0	27.45	0.813	0.276	364.8
	LoD 7	2497	27.42	0.811	0.268	73.7	27.47	0.814	0.269	590.6
Ours 3DGS-MCMC	LoD 0	100	25.40	0.718	0.406	3.7	25.26	0.718	0.407	23.7
	LoD 1	155	26.22	0.750	0.370	5.6	26.15	0.752	0.369	35.9
	LoD 2	242	26.75	0.775	0.338	8.4	26.77	0.779	0.334	56.3
	LoD 3	381	27.12	0.794	0.310	12.9	27.23	0.800	0.305	89.0
	LoD 4	603	27.37	0.806	0.288	19.9	27.52	0.814	0.280	141.5
	LoD 5	962	27.50	0.814	0.271	30.8	27.69	0.823	0.262	226.5
	LoD 6	1546	27.55	0.817	0.261	47.3	27.74	0.826	0.252	364.8
	LoD 7	2497	27.55	0.819	0.257	72.2	27.74	0.827	0.248	590.6
Ours Scaffold-GS	LoD 0	50	24.97	0.710	0.409	4.0	25.03	0.711	0.408	15.1
	LoD 1	68	25.98	0.743	0.375	5.4	26.03	0.744	0.374	20.7
	LoD 2	94	26.68	0.768	0.345	7.4	26.72	0.769	0.344	28.6
	LoD 3	129	27.24	0.789	0.318	10.2	27.27	0.790	0.317	39.5
	LoD 4	179	27.61	0.803	0.297	14.1	27.63	0.804	0.296	54.3
	LoD 5	248	27.77	0.810	0.284	19.6	27.81	0.811	0.283	75.7
	LoD 6	346	27.84	0.812	0.278	27.2	27.88	0.813	0.277	104.9
	LoD 7	483	27.87	0.813	0.276	37.9	27.89	0.814	0.275	146.2
Ours Octree-GS	LoD 0	50	24.61	0.689	0.426	3.7	24.63	0.690	0.425	14.7
	LoD 1	69	25.55	0.722	0.391	5.2	25.57	0.723	0.390	20.2
	LoD 2	96	26.33	0.752	0.357	7.1	26.36	0.753	0.356	28.1
	LoD 3	133	27.01	0.780	0.322	10.0	27.05	0.781	0.321	39.1
	LoD 4	186	27.49	0.802	0.291	13.9	27.53	0.802	0.291	54.7
	LoD 5	262	27.73	0.813	0.271	19.5	27.78	0.814	0.270	77.0
	LoD 6	371	27.85	0.818	0.260	27.5	27.89	0.818	0.260	108.9
	LoD 7	527	27.87	0.818	0.257	39.0	27.91	0.819	0.257	154.7

Table 5. Compressed vs Not Compressed models on Tanks&Temples.

Method	LoD	W	Compressed				Not Compressed			
			PSNR \uparrow	SSIM \uparrow	LPIPS \downarrow	Size[MB] \downarrow	PSNR \uparrow	SSIM \uparrow	LPIPS \downarrow	Size[MB] \downarrow
Ours 3DGS	LoD 0	100	21.82	0.770	0.330	3.6	21.84	0.775	0.323	23.7
	LoD 1	144	22.62	0.795	0.302	5.0	22.64	0.801	0.295	34.0
	LoD 2	208	23.12	0.813	0.278	7.0	23.17	0.819	0.271	49.1
	LoD 3	301	23.46	0.826	0.258	9.7	23.55	0.832	0.251	71.2
	LoD 4	438	23.65	0.834	0.244	13.6	23.75	0.841	0.236	103.6
	LoD 5	639	23.73	0.838	0.235	19.2	23.83	0.845	0.227	151.2
	LoD 6	936	23.75	0.840	0.230	26.6	23.87	0.847	0.222	221.5
	LoD 7	1376	23.75	0.841	0.227	36.8	23.87	0.848	0.219	325.5
Ours 3DGS-MCMC	LoD 0	100	21.92	0.769	0.333	3.5	21.74	0.771	0.328	23.7
	LoD 1	144	22.69	0.793	0.303	4.9	22.55	0.796	0.296	34.0
	LoD 2	208	23.22	0.812	0.278	6.8	23.14	0.816	0.269	49.1
	LoD 3	301	23.62	0.826	0.255	9.5	23.61	0.832	0.245	71.2
	LoD 4	438	23.85	0.836	0.238	13.3	23.89	0.844	0.226	103.6
	LoD 5	640	23.99	0.841	0.226	18.7	24.06	0.851	0.212	151.2
	LoD 6	938	24.04	0.845	0.217	26.6	24.11	0.854	0.203	221.5
	LoD 7	1380	24.05	0.845	0.215	37.4	24.12	0.856	0.197	325.5
Ours Scaffold-GS	LoD 0	50	23.13	0.806	0.295	3.9	23.13	0.806	0.295	15.1
	LoD 1	61	23.51	0.821	0.273	4.8	23.51	0.821	0.273	18.5
	LoD 2	75	23.72	0.832	0.256	5.9	23.74	0.832	0.256	22.8
	LoD 3	93	23.86	0.839	0.242	7.3	23.88	0.839	0.242	28.0
	LoD 4	114	23.96	0.844	0.231	8.9	23.98	0.844	0.231	34.5
	LoD 5	141	24.01	0.848	0.224	11.0	24.04	0.848	0.224	42.5
	LoD 6	174	24.04	0.850	0.219	13.5	24.07	0.850	0.220	53.7
	LoD 7	215	24.04	0.851	0.218	16.6	24.07	0.851	0.218	65.5
Ours Octree-GS	LoD 0	50	23.08	0.798	0.342	3.9	23.10	0.800	0.340	14.7
	LoD 1	68	23.68	0.819	0.312	5.3	23.70	0.820	0.310	20.0
	LoD 2	93	24.01	0.834	0.286	7.1	24.03	0.840	0.280	27.3
	LoD 3	127	24.25	0.847	0.262	9.7	24.26	0.850	0.260	37.2
	LoD 4	173	24.40	0.856	0.242	13.2	24.42	0.860	0.240	50.7
	LoD 5	235	24.50	0.863	0.227	17.9	24.52	0.860	0.230	69.2
	LoD 6	321	24.56	0.867	0.218	24.2	24.58	0.870	0.220	94.3
	LoD 7	438	24.56	0.868	0.215	32.8	24.59	0.870	0.210	128.6

Table 6. Compressed vs Not Compressed models on DeepBlending.

Method	LoD	W	Compressed				Not Compressed			
			PSNR \uparrow	SSIM \uparrow	LPIPS \downarrow	Size[MB] \downarrow	PSNR \uparrow	SSIM \uparrow	LPIPS \downarrow	Size[MB] \downarrow
Ours 3DGS	LoD 0	100	29.22	0.888	0.372	3.7	29.01	0.888	0.373	23.7
	LoD 1	137	29.57	0.896	0.358	5.3	29.44	0.897	0.355	36.5
	LoD 2	189	29.70	0.900	0.348	7.4	29.60	0.902	0.343	56.3
	LoD 3	259	29.78	0.902	0.339	10.5	29.62	0.905	0.334	87.0
	LoD 4	357	29.78	0.904	0.333	14.8	29.60	0.905	0.328	134.5
	LoD 5	491	29.78	0.904	0.328	20.7	29.58	0.905	0.324	208.1
	LoD 6	676	29.77	0.905	0.325	28.9	29.55	0.905	0.322	322.0
	LoD 7	931	29.77	0.905	0.324	39.8	29.54	0.904	0.322	498.6
Ours 3DGS-MCMC	LoD 0	100	29.12	0.887	0.376	3.6	28.95	0.888	0.373	23.7
	LoD 1	137	29.44	0.894	0.361	5.0	29.41	0.896	0.356	36.5
	LoD 2	189	29.59	0.898	0.350	7.0	29.58	0.901	0.343	56.3
	LoD 3	259	29.65	0.900	0.342	9.8	29.63	0.903	0.333	87.0
	LoD 4	357	29.70	0.902	0.335	13.6	29.64	0.904	0.326	134.5
	LoD 5	491	29.72	0.902	0.329	19.1	29.62	0.904	0.321	208.1
	LoD 6	676	29.73	0.903	0.326	26.7	29.58	0.904	0.319	322.0
	LoD 7	931	29.71	0.902	0.325	37.5	29.55	0.903	0.318	498.6
Ours Scaffold-GS	LoD 0	50	29.76	0.897	0.359	3.9	29.73	0.896	0.360	15.1
	LoD 1	58	30.02	0.901	0.350	4.5	29.97	0.900	0.351	17.6
	LoD 2	68	30.16	0.904	0.344	5.3	30.11	0.903	0.345	20.5
	LoD 3	80	30.26	0.906	0.339	6.2	30.20	0.905	0.340	24.0
	LoD 4	93	30.31	0.908	0.335	7.2	30.27	0.907	0.336	28.2
	LoD 5	109	30.36	0.909	0.332	8.4	30.31	0.907	0.333	34.0
	LoD 6	127	30.38	0.909	0.330	9.8	30.33	0.908	0.331	38.7
	LoD 7	149	30.38	0.909	0.329	11.4	30.31	0.908	0.330	46.0
Ours Octree-GS	LoD 0	50	29.67	0.895	0.358	3.6	29.72	0.895	0.358	14.7
	LoD 1	56	29.87	0.898	0.352	4.0	29.92	0.898	0.351	16.6
	LoD 2	64	29.98	0.900	0.348	4.5	30.04	0.900	0.347	18.7
	LoD 3	72	30.04	0.901	0.344	5.1	30.10	0.901	0.343	21.1
	LoD 4	81	30.07	0.902	0.341	5.7	30.13	0.902	0.341	23.7
	LoD 5	91	30.10	0.902	0.339	6.5	30.15	0.903	0.339	26.8
	LoD 6	103	30.10	0.902	0.338	7.3	30.16	0.903	0.337	30.2
	LoD 7	116	30.11	0.902	0.337	8.2	30.16	0.903	0.337	34.0

Table 7. Hyperparameters used for deriving the rate/distortion curves for the given methods. Notation is in accordance with the respective papers.

Method	Compression Rate		
	High	Medium	Low
HAC [7]	$\lambda = 0.01$	$\lambda = 0.001$	$\lambda = 0.005$
RDO [37]	$\lambda_{sh} = 0.05, \lambda_{gs} = 0.005$	$\lambda_{sh} = 0.02, \lambda_{gs} = 0.002$	$\lambda_{sh} = 0.005, \lambda_{gs} = 0.0005$
Reduced-3DGS [33]	$\tau_{std} = 0.06, \tau_{cdist} = 8$	$\tau_{std} = 0.04, \tau_{cdist} = 6$	$\tau_{std} = 0.01, \tau_{cdist} = 1$
Comp-GS [23]	$\lambda = 0.01$	$\lambda = 0.001$	$\lambda = 0.005$
SoG [27]	with SH	-	no SHs

For SOG, we identify with *low* and *high* the version with SHs and without SHs, respectively. In Tab. 8 all the results for each dataset are reported (this is the complete version of Tab. 1). Notably, our method is the only one trained once, meaning that the curves are generated instantly without the need for re-training.

10.2. LoD Visualizations

In Fig. 10, 11, 12 we show all LoD levels for each dataset on 3DGS. We observe that the transition between levels is smooth, with each level progressively adding more detail without introducing artifacts. We observe that lower levels exhibit a loss of detail in high-frequency regions, particularly in background areas. Examples include the trees in the *bicycle* scene, the details of the building in the background of the *garden* scene, and the reflections and

transparencies in the background of the *counter* scene.

10.3. Per Scene Results

In Tab. 11, 9, 10 we provide per-scene results for all 3 tested models across every LoD level with compression, along with the corresponding baseline values.

Table 8. Main results on the 3 dataset (Mip-Nerf360, Tanks&Temples and DeepBlending). All results were tested on a NVIDIA A40.

	Dataset Method/Metric	Mip-Nerf360						Tanks&Temples						Deep Blending					
		PSNR \uparrow	SSIM \uparrow	LPIPS \downarrow	Size[MB] \downarrow	W \downarrow	FPS \uparrow	PSNR \uparrow	SSIM \uparrow	LPIPS \downarrow	Size[MB] \downarrow	W \downarrow	FPS \uparrow	PSNR \uparrow	SSIM \uparrow	LPIPS \downarrow	Size[MB] \downarrow	W \downarrow	FPS \uparrow
Ours 3DGS	LoD 0	25.28	0.719	0.407	3.8	100	548	21.82	0.770	0.330	3.6	100	627	29.22	0.888	0.372	3.7	100	814
	LoD 1	26.10	0.751	0.371	5.6	155	457	22.62	0.795	0.302	5.0	144	542	29.57	0.896	0.358	5.3	146	717
	LoD 2	26.63	0.776	0.341	8.6	242	391	23.12	0.813	0.278	7.0	208	470	29.70	0.900	0.348	7.4	212	622
	LoD 3	27.05	0.793	0.314	13.3	381	333	23.46	0.826	0.258	9.7	301	394	29.78	0.902	0.339	10.5	309	540
	LoD 4	27.30	0.804	0.293	20.6	603	282	23.65	0.834	0.244	13.6	437	337	29.78	0.904	0.333	14.8	451	465
	LoD 5	27.40	0.809	0.278	32.1	962	236	23.73	0.838	0.235	19.2	638	278	29.78	0.904	0.328	20.7	658	395
	LoD 6	27.43	0.811	0.271	49.0	1546	197	23.75	0.840	0.230	26.6	935	230	29.77	0.905	0.325	28.9	962	327
	LoD 7	27.42	0.811	0.268	73.7	2497	175	23.75	0.841	0.227	36.8	1374	205	29.77	0.905	0.324	39.8	1406	270
baseline	27.48	0.816	0.256	787.0	3329	148	23.79	0.849	0.213	434.0	1840	186	29.46	0.904	0.314	665.0	2811	167	
Ours 3DGS-MCMC	LoD 0	25.40	0.718	0.406	3.7	100	409	21.92	0.769	0.333	3.5	100	510	29.12	0.887	0.376	3.6	100	633
	LoD 1	26.22	0.750	0.370	5.6	155	348	22.69	0.793	0.303	4.9	144	427	29.44	0.894	0.361	5.0	146	537
	LoD 2	26.75	0.775	0.338	8.4	242	299	23.22	0.812	0.278	6.8	208	359	29.59	0.898	0.350	7.0	212	459
	LoD 3	27.12	0.794	0.310	12.9	381	255	23.62	0.826	0.255	9.5	301	307	29.65	0.900	0.342	9.8	310	422
	LoD 4	27.37	0.806	0.288	19.9	603	214	23.85	0.836	0.238	13.3	438	246	29.70	0.902	0.335	13.6	452	356
	LoD 5	27.50	0.814	0.271	30.8	962	176	23.99	0.841	0.226	18.7	640	206	29.72	0.902	0.329	19.1	660	312
	LoD 6	27.55	0.817	0.261	47.3	1546	143	24.04	0.845	0.217	26.6	938	178	29.73	0.903	0.326	26.7	965	267
	LoD 7	27.55	0.819	0.257	72.2	2497	123	24.05	0.845	0.215	37.4	1379	163	29.71	0.902	0.325	37.5	1411	229
baseline	27.84	0.831	0.239	794.0	3528	87	24.15	0.862	0.187	435.0	1840	133	29.65	0.904	0.309	667.0	2822	164	
Ours Scaffold-GS	LoD 0	24.97	0.710	0.409	4.0	50	145	23.13	0.806	0.295	3.9	50	177	29.76	0.897	0.359	3.9	50	184
	LoD 1	25.98	0.743	0.375	5.4	68	135	23.51	0.821	0.273	4.8	61	162	30.02	0.901	0.350	4.5	58	180
	LoD 2	26.68	0.768	0.345	7.4	94	122	23.72	0.832	0.256	5.9	75	150	30.16	0.904	0.344	5.3	68	173
	LoD 3	27.24	0.789	0.318	10.2	129	108	23.86	0.839	0.242	7.3	93	134	30.26	0.906	0.339	6.2	80	168
	LoD 4	27.61	0.803	0.297	14.1	179	94	23.96	0.844	0.231	8.9	114	128	30.31	0.908	0.335	7.2	93	166
	LoD 5	27.77	0.810	0.284	19.6	248	84	24.01	0.848	0.224	11.0	141	116	30.36	0.909	0.332	8.4	109	163
	LoD 6	27.84	0.812	0.278	27.2	346	75	24.04	0.850	0.219	13.5	174	109	30.38	0.909	0.330	9.8	127	159
	LoD 7	27.87	0.813	0.276	37.9	483	69	24.04	0.851	0.218	16.6	215	100	30.38	0.909	0.329	11.4	149	158
baseline	27.77	0.813	0.270	171.0	555	79	24.03	0.853	0.210	76.0	247	108	30.28	0.909	0.318	53.0	171	179	
Ours Octree-GS	LoD 0	24.61	0.689	0.426	3.7	50	123	23.08	0.798	0.342	3.9	50	94	29.67	0.895	0.358	3.6	50	150
	LoD 1	25.55	0.722	0.391	5.2	69	114	23.68	0.819	0.312	5.3	68	86	29.87	0.898	0.352	4.0	56	146
	LoD 2	26.33	0.752	0.357	7.1	96	104	24.01	0.834	0.286	7.1	93	78	29.98	0.900	0.348	4.5	64	146
	LoD 3	27.01	0.780	0.322	10.0	133	92	24.25	0.847	0.262	9.7	127	72	30.04	0.901	0.344	5.1	72	142
	LoD 4	27.49	0.802	0.291	13.9	186	81	24.40	0.856	0.242	13.2	173	65	30.07	0.902	0.341	5.7	81	139
	LoD 5	27.73	0.813	0.271	19.5	262	71	24.50	0.863	0.227	17.9	235	57	30.10	0.902	0.339	6.5	91	140
	LoD 6	27.85	0.818	0.260	27.5	371	64	24.56	0.867	0.218	24.2	321	51	30.10	0.902	0.338	7.3	103	135
	LoD 7	27.87	0.818	0.257	39.0	527	60	24.56	0.868	0.215	32.8	438	45	30.11	0.902	0.337	8.2	116	135
baseline	27.96	0.821	0.252	157.2	606	69	24.69	0.873	0.204	131.0	503	49	30.09	0.902	0.338	34.6	133	174	
HAC [7]	high	27.17	0.798	0.306	11.5	371	74	24.03	0.843	0.237	7.4	261	82	29.92	0.903	0.250	3.9	180	166
	medium	27.53	0.807	0.290	15.2	425	72	24.05	0.846	0.222	7.9	300	85	29.98	0.904	0.340	4.1	187	173
	low	27.78	0.812	0.277	22.0	501	68	24.37	0.853	0.215	11.1	307	88	30.34	0.909	0.329	6.3	196	166
RDO [37]	high	26.45	0.782	0.322	9.7	862	280	23.19	0.827	0.253	5.5	395	370	29.61	0.903	0.331	7.0	531	335
	medium	26.89	0.796	0.298	15.3	1236	227	23.16	0.833	0.239	8.0	598	307	29.68	0.905	0.323	11.0	891	269
	low	27.05	0.801	0.288	23.3	1860	178	23.32	0.839	0.232	11.9	912	257	29.72	0.906	0.318	18.0	1478	200
Reduced-3DGS [33]	high	27.05	0.807	0.272	22.7	1245	247	23.46	0.840	0.228	10.5	558	384	29.63	0.906	0.318	13.6	804	337
	medium	27.19	0.810	0.267	29.3	1436	234	23.55	0.843	0.223	14.0	656	358	29.70	0.907	0.315	18.3	990	304
	low	27.28	0.813	0.264	45.8	1434	240	23.57	0.844	0.221	20.7	648	360	29.69	0.907	0.314	35.3	988	311
Comp-GS [23]	high	26.40	0.778	0.323	9.0	454	233	23.06	0.816	0.278	6.1	270	334	29.22	0.894	0.369	6.0	311	440
	medium	26.71	0.790	0.305	10.9	470	193	23.32	0.828	0.259	7.3	242	311	29.56	0.899	0.351	7.1	271	315
	low	27.28	0.802	0.283	16.4	485	165	23.62	0.837	0.248	9.8	241	286	29.89	0.904	0.336	10.0	246	254
SOG [28]	high	26.56	0.791	0.241	16.7	2150	119	23.15	0.828	0.198	9.3	1207	216	29.12	0.892	0.270	9.3	800	219
	low	27.08	0.799	0.230	40.3	2176	132	23.56	0.837	0.186	22.8	1242	227	29.26	0.894	0.268	17.7	890	236
EAGLES [15]	-	27.13	0.809	0.278	57.1	1290	156	23.20	0.837	0.241	28.9	651	227	29.75	0.910	0.318	52.4	1192	144
LightGaussian [11]	-	27.24	0.810	0.273	51.0	2197	161	23.55	0.839	0.235	28.5	1211	225	29.41	0.904	0.329	43.2	956	348
Compact-3DGS [22]	-	27.02	0.800	0.287	29.1	1429	108	23.41	0.836	0.238	20.9	842	147	29.76	0.905	0.324	23.8	1053	144

Table 9. Per-scene results on Tanks&Temples.

Scene	Method/Metric	Ours 3DGS						Ours 3DGS-MCMC						Ours Scaffold-GS						Ours Octree-GS					
		PSNR \uparrow	SSIM \uparrow	LPIPS \downarrow	W \downarrow	MB \downarrow	FPS \downarrow	PSNR \uparrow	SSIM \uparrow	LPIPS \downarrow	W \downarrow	MB \downarrow	FPS \downarrow	PSNR \uparrow	SSIM \uparrow	LPIPS \downarrow	W \downarrow	MB \downarrow	FPS \downarrow	PSNR \uparrow	SSIM \uparrow	LPIPS \downarrow	W \downarrow	MB \downarrow	FPS \downarrow
Train	baseline	22.19	0.815	0.249	1088	257.3	197	22.30	0.828	0.238	1090	258.0	141	22.23	0.820	0.246	196	60.5	107	22.80	0.848	0.233	526	136.0	44
	LoD 7	22.09	0.800	0.274	812	23.0	196	22.26	0.802	0.278	816	22.3	199	22.31	0.818	0.257	171	13.0	105	22.70	0.842	0.246	458	35.4	41
	LoD 6	22.08	0.799	0.280	602	17.6	234	22.26	0.802	0.278	604	17.2	213	22.30	0.817	0.260	143	10.9	114						

Table 10. Per-scene results on DeepBlending.

Scene	Method/Metric LoD	Ours 3DGS						Ours 3DGS-MCMC						Ours Scaffold-GS						Ours Octree-GS					
		PSNR \uparrow	SSIM \uparrow	LPIPS \downarrow	W \downarrow	MB \downarrow	FPS \downarrow	PSNR \uparrow	SSIM \uparrow	LPIPS \downarrow	W \downarrow	MB \downarrow	FPS \downarrow	PSNR \uparrow	SSIM \uparrow	LPIPS \downarrow	W \downarrow	MB \downarrow	FPS \downarrow	PSNR \uparrow	SSIM \uparrow	LPIPS \downarrow	W \downarrow	MB \downarrow	FPS \downarrow
DrJohnson	baseline	29.03	0.900	0.318	3298	780.1	146	28.92	0.892	0.320	3308	782.0	173	29.75	0.907	0.322	192	59.2	167	29.20	0.894	0.350	140	162.4	140
	LoD 7	29.28	0.899	0.332	1649	47.9	316	29.00	0.892	0.338	1654	45.1	290	29.76	0.91	0.33	167	12.6	148	29.27	0.894	0.348	122	8.6	130
	LoD 6	29.27	0.899	0.333	1105	34.1	389	29.00	0.892	0.340	1108	31.5	335	29.73	0.91	0.33	141	10.6	151	29.25	0.894	0.349	107	7.6	130
	LoD 5	29.28	0.898	0.337	740	23.9	482	28.98	0.892	0.344	742	21.9	398	29.70	0.905	0.337	118	9.0	154	29.25	0.894	0.350	95	6.7	134
	LoD 4	29.26	0.897	0.342	496	16.6	570	28.97	0.891	0.350	497	15.2	457	29.64	0.903	0.340	100	7.6	158	29.23	0.893	0.352	83	5.9	133
	LoD 3	29.25	0.895	0.350	332	11.4	679	28.87	0.889	0.358	333	10.8	553	29.57	0.901	0.346	84	6.4	163	29.21	0.892	0.355	73	5.2	136
	LoD 2	29.15	0.891	0.361	223	7.9	767	28.77	0.885	0.368	223	7.4	593	29.45	0.898	0.352	71	5.4	171	29.15	0.891	0.359	65	4.6	140
	LoD 1	28.98	0.886	0.374	149	5.4	867	28.58	0.880	0.381	149	5.2	681	29.28	0.894	0.360	59	4.5	176	29.05	0.89	0.36	57	4.1	142
LoD 0	28.56	0.875	0.391	100	3.7	970	28.17	0.871	0.399	100	3.6	818	28.97	0.888	0.370	50	3.8	179	28.85	0.89	0.37	50	3.6	144	
Playroom	baseline	29.89	0.907	0.309	2324	550	187	30.39	0.916	0.298	2335	552.0	154	30.81	0.912	0.314	150	46.2	190	30.99	0.911	0.326	126	32.6	186
	LoD 7	30.27	0.911	0.316	1162	31.7	224	30.43	0.913	0.311	1168	30.0	168	30.99	0.912	0.325	130	10.2	168	30.95	0.911	0.327	110	7.8	141
	LoD 6	30.27	0.911	0.317	818	23.7	266	30.46	0.913	0.311	822	21.9	198	31.02	0.912	0.326	114	8.9	166	30.95	0.911	0.327	98	6.9	141
	LoD 5	30.28	0.911	0.320	577	17.5	308	30.45	0.913	0.315	579	16.2	225	31.01	0.912	0.327	99	7.8	172	30.94	0.911	0.329	88	6.2	145
	LoD 4	30.29	0.911	0.324	406	13.0	359	30.43	0.913	0.320	407	12.0	255	30.98	0.912	0.329	86	6.8	174	30.91	0.910	0.330	78	5.6	145
	LoD 3	30.30	0.910	0.328	286	9.5	402	30.43	0.912	0.325	287	8.8	290	30.94	0.911	0.332	75	6.0	173	30.87	0.910	0.333	70	5.0	149
	LoD 2	30.25	0.909	0.334	202	7.0	477	30.40	0.911	0.333	202	6.6	326	30.87	0.910	0.336	66	5.2	175	30.82	0.909	0.336	63	4.5	151
	LoD 1	30.15	0.906	0.342	142	5.1	566	30.31	0.908	0.341	142	4.8	392	30.77	0.908	0.340	57	4.5	183	30.70	0.907	0.340	56	4.0	149
LoD 0	29.89	0.901	0.354	100	3.8	658	30.07	0.904	0.353	100	3.6	449	30.56	0.905	0.347	50	4.0	189	30.50	0.905	0.346	50	3.6	156	



Figure 10. Full LoD visualization with 3DGS on *Tanks&Temples* dataset.



Figure 11. Full LoD visualization with 3DGS on *DeepBlending* dataset.

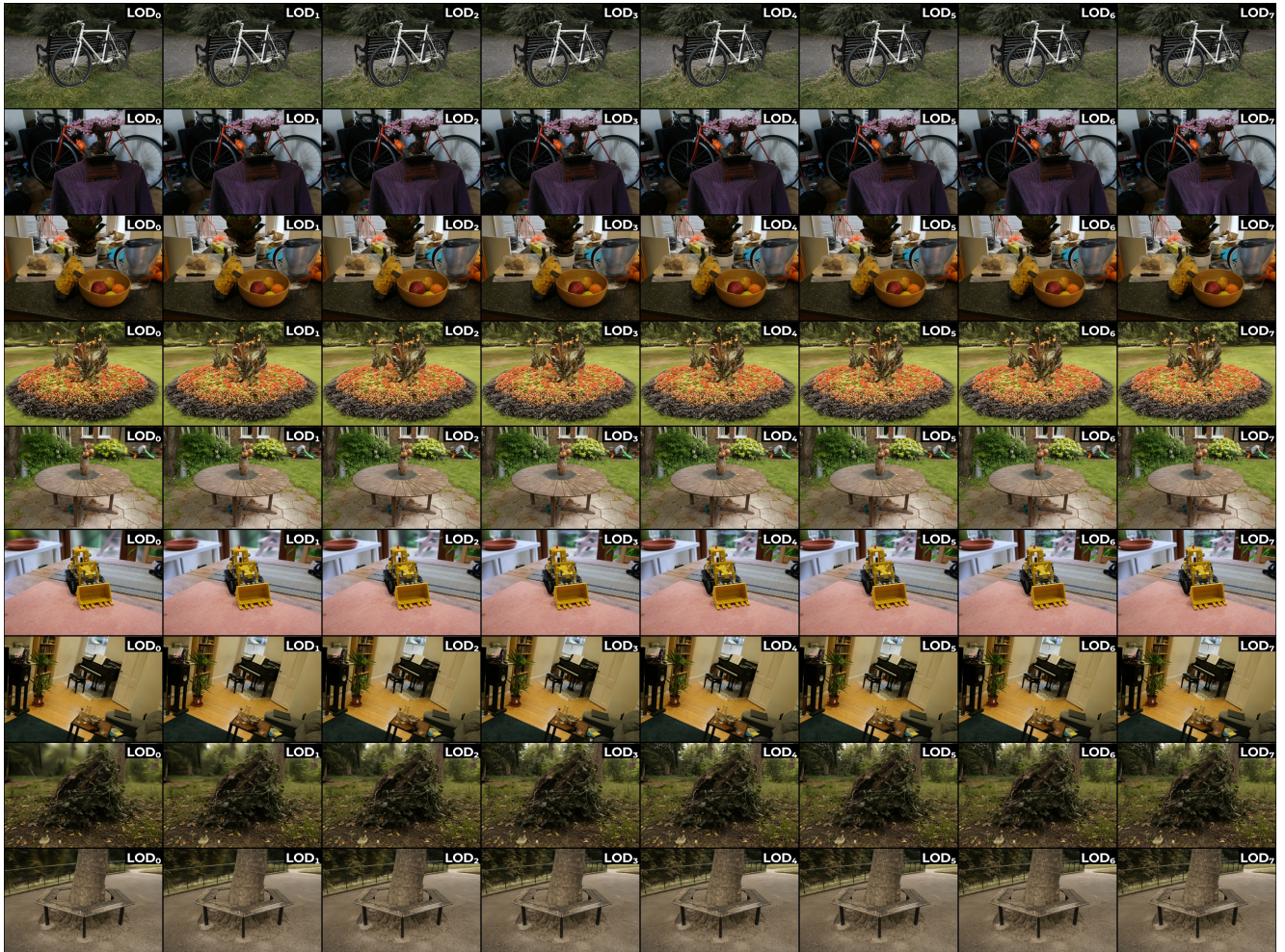


Figure 12. Full LoD visualization with 3DGS on *Mip-NeRF360* dataset.

Table 11. Per-scene results on Mip-NeRF360.

Scene	Method/Metric LoD	Ours 3DGS						Ours 3DGS-MCMC						Ours Scaffold-GS						Ours Octree-GS					
		PSNR↑	SSIM↑	LPIPS↓	W↓	MB↓	FPS↑	PSNR↑	SSIM↑	LPIPS↓	W↓	MB↓	FPS↑	PSNR↑	SSIM↑	LPIPS↓	W↓	MB↓	FPS↑	PSNR↑	SSIM↑	LPIPS↓	W↓	MB↓	FPS↑
Bicycle	baseline	25.17	0.765	0.24	6091	1371	89	25.53	0.791	0.211	6091	1371	60	25.18	0.747	0.289	879	749.0	60	25.31	0.761	0.256	1049	273.8	52
	LoD 7	25.04	0.757	0.254	4569	134.0	141	25.24	0.770	0.236	4569	130.0	110	25.27	0.748	0.291	764	60.3	51	25.16	0.758	0.260	912	67.8	45
	LoD 6	25.04	0.756	0.258	2646	84.3	170	25.23	0.770	0.240	2646	81.2	131	25.25	0.748	0.293	518	40.8	54	25.18	0.757	0.263	602	44.9	47
	LoD 5	25.00	0.752	0.273	1533	51.3	226	25.16	0.760	0.261	1533	48.9	177	25.22	0.745	0.300	351	27.9	61	25.09	0.749	0.279	398	29.9	53
	LoD 4	24.89	0.742	0.297	888	30.3	286	24.98	0.750	0.290	888	29.1	232	25.01	0.728	0.326	238	18.9	75	24.74	0.721	0.320	263	19.9	63
	LoD 3	24.68	0.724	0.327	514	17.8	353	24.68	0.720	0.326	514	17.3	287	24.67	0.703	0.357	161	12.9	87	24.20	0.675	0.374	174	13.2	74
	LoD 2	24.34	0.694	0.365	298	10.4	425	24.32	0.690	0.370	298	10.3	357	24.20	0.669	0.393	109	8.8	101	23.69	0.630	0.421	115	8.7	89
	LoD 1	23.85	0.653	0.411	173	6.1	503	23.81	0.650	0.417	173	6.1	421	23.59	0.629	0.430	74	5.9	113	23.17	0.591	0.460	76	5.8	102
LoD 0	23.11	0.599	0.461	100	3.6	625	23.11	0.590	0.466	100	3.6	478	22.69	0.582	0.470	50	4.0	125	22.50	0.551	0.496	50	3.8	110	
Bonsai	baseline	32.20	0.942	0.253	1258	283	215	32.32	0.943	0.261	1258	283	106	32.80	0.949	0.233	400	524.0	75	32.79	0.949	0.236	240	62.4	106
	LoD 7	31.89	0.939	0.266	944	25.8	211	31.92	0.940	0.265	944	25.6	154	32.95	0.950	0.242	348	25.5	69	32.72	0.948	0.238	209	14.2	89
	LoD 6	31.89	0.939	0.266	685	19.6	225	31.91	0.940	0.265	685	18.8	159	32.90	0.950	0.243	264	19.5	74	32.71	0.947	0.240	170	11.7	92
	LoD 5	31.83	0.938	0.268	497	14.8	245	31.87	0.940	0.270	497	14.3	182	32.82	0.948	0.246	200	14.8	86	32.60	0.946	0.243	139	9.6	99
	LoD 4	31.77	0.937	0.273	361	11.3	276	31.76	0.940	0.277	361	10.8	207	32.58	0.945	0.252	152	11.3	100	32.36	0.942	0.250	113	7.8	105
	LoD 3	31.67	0.935	0.281	262	8.6	296	31.59	0.930	0.286	262	8.2	230	32.09	0.939	0.263	115	8.6	113	31.80	0.935	0.262	92	6.4	112
	LoD 2	31.39	0.930	0.292	190	6.4	338	31.28	0.930	0.299	190	6.2	259	31.26	0.929	0.281	87	6.5	128	30.83	0.924	0.280	75	5.2	119
	LoD 1	30.85	0.922	0.307	138	4.8	379	30.73	0.920	0.316	138	4.8	290	30.18	0.913	0.304	66	4.9	142	29.58	0.908	0.304	61	4.3	124
LoD 0	29.69	0.906	0.330	100	3.7	434	29.54	0.900	0.339	100	3.6	311	28.44	0.887	0.338	50	3.8	154	28.18	0.887	0.331	50	3.5	135	
Counter	baseline	29.01	0.909	0.258	1205	271	150	28.95	0.911	0.257	1205	271	82	29.67	0.918	0.242	273	383.0	73	30.20	0.925	0.232	336	86.4	63
	LoD 7	28.86	0.904	0.271	904	25.2	158	28.80	0.900	0.269	904	24.9	119	29.85	0.919	0.249	238	17.3	70	30.08	0.924	0.236	292	19.5	56
	LoD 6	28.87	0.904	0.272	660	19.3	170	28.80	0.900	0.270	660	18.8	128	29.80	0.918	0.252	190	14.0	75	30.04	0.922	0.242	227	15.3	60
	LoD 5	28.86	0.904	0.274	482	15.0	186	28.79	0.900	0.273	482	14.5	148	29.72	0.915	0.260	152	11.3	82	29.91	0.917	0.254	176	12.0	68
	LoD 4	28.83	0.902	0.279	352	11.5	206	28.73	0.900	0.279	352	11.3	163	29.55	0.909	0.272	122	9.0	89	29.68	0.908	0.271	137	9.3	74
	LoD 3	28.74	0.899	0.288	257	8.8	221	28.62	0.900	0.288	257	8.6	179	29.26	0.900	0.288	97	7.2	96	29.28	0.896	0.292	107	7.3	81
	LoD 2	28.54	0.893	0.299	188	6.6	247	28.45	0.890	0.299	188	6.6	196	28.79	0.887	0.308	78	5.8	103	28.67	0.881	0.315	83	5.7	87
	LoD 1	28.21	0.885	0.314	137	5.0	281	28.19	0.880	0.314	137	5.0	225	28.21	0.872	0.330	62	4.7	111	27.97	0.864	0.339	64	4.4	94
LoD 0	27.61	0.871	0.334	100	3.8	329	27.61	0.870	0.334	100	3.8	255	27.43	0.853	0.354	50	3.7	119	27.09	0.844	0.365	50	3.4	103	
Flowers	baseline	21.54	0.606	0.366	3598	810	178	21.96	0.638	0.324	3598	810	77	21.25	0.577	0.407	669	592.0	90	21.52	0.599	0.375	777	202.4	70
	LoD 7	21.44	0.596	0.378	2698	80.7	231	21.65	0.610	0.350	2698	82.2	118	21.27	0.579	0.408	582	47.6	80	21.51	0.598	0.377	676	52.8	61
	LoD 6	21.44	0.595	0.382	1653	54.7	252	21.62	0.610	0.362	1653	53.1	151	21.27	0.579	0.410	410	33.7	88	21.51	0.597	0.379	466	36.6	67
	LoD 5	21.42	0.592	0.392	1053	36.0	305	21.54	0.600	0.376	1053	35.4	199	21.27	0.577	0.414	289	23.9	97	21.49	0.594	0.386	321	25.5	74
	LoD 4	21.35	0.584	0.408	657	23.1	358	21.36	0.580	0.398	657	22.5	248	21.21	0.572	0.422	203	16.9	107	21.37	0.585	0.399	221	17.7	84
	LoD 3	21.19	0.569	0.428	411	14.8	438	21.10	0.560	0.423	411	14.4	304	20.93	0.556	0.439	143	12.0	125	21.02	0.563	0.421	153	12.3	99
	LoD 2	20.89	0.543	0.453	256	9.5	496	20.77	0.530	0.450	256	9.3	358	20.51	0.532	0.459	101	8.5	143	20.33	0.528	0.451	105	8.5	118
	LoD 1	20.44	0.510	0.480	160	6.0	565	20.29	0.490	0.479	160	5.9	430	20.02	0.504	0.481	71	6.0	160	19.55	0.487	0.483	73	5.9	137
LoD 0	19.76	0.470	0.511	100	3.9	703	19.58	0.450	0.513	100	3.8	493	19.38	0.470	0.506	50	4.2	173	18.75	0.444	0.517	50	4.1	146	
Garden	baseline	27.39	0.867	0.123	5872	1322	100	27.68	0.874	0.114	5872	1322	76	27.28	0.850	0.157	732	1111.0	58	27.61	0.860	0.134	856	220.0	44
	LoD 7	27.21	0.859	0.139	4404	133.2	126	27.31	0.860	0.135	4404	126.4	107	27.19	0.845	0.167	636	50.0	52	27.52	0.854	0.147	744	57.0	39
	LoD 6	27.20	0.859	0.142	2564	85.2	160	27.29	0.860	0.139	2564	80.4	141	27.15	0.844	0.172	443	35.1	60	27.42	0.850	0.154	506	39.1	45
	LoD 5	27.11	0.854	0.156	1493	52.7	218	27.16	0.850	0.155	1493	50.0	193	26.94	0.835	0.188	308	24.6	73	27.12	0.837	0.178	344	26.7	56
	LoD 4	26.79	0.840	0.187	870	31.5	284	26.78	0.840	0.188	870	30.3	249	26.58	0.817	0.219	214	17.2	91	26.66	0.813	0.219	234	18.2	71
	LoD 3	26.02	0.807	0.241	506	18.6	355	26.11	0.810	0.240	506	18.2	309	25.97	0.788	0.262	149	12.0	109	25.94	0.775	0.277	159	12.4	85
	LoD 2	24.95	0.755	0.308	295	11.0	447	25.09	0.760	0.305	295	10.6	374	25.06	0.745	0.315	103	8.4	130	24.92	0.723	0.336	108	8.5	103
	LoD 1	23.84	0.691	0.373	172	6.4	543	23.98	0.700	0.371	172	6.3	449	24.06	0.694	0.368	72	5.8	149	23.85	0.664	0.391	74	5.8	115
LoD 0	22.66	0.619	0.436	100	3.9	682	22.83	0.620	0.436	100	3.7	552	22.71	0.633	0.421	50	4.1	164	22.55	0.598	0.442	50	3.9	124	
Kitchen	baseline	31.51	0.928	0.155	1827	411	122	31.83	0.929	0.162	1827	411	76	31.81	0.932	0.146	332	879.0	57	31.99	0.934	0.145	319	82.3	55
	LoD 7	31.40	0.924	0.166	1371	38.6	136	31.16	0.920	0.176	1371	36.1	111	31.81	0.931	0.153	289	22.2	54	31.58	0.931	0.152	278	19.7	51
	LoD 6	31.43	0.924	0.167	943	28.1	161	31.15	0.920	0.177	943	25.9	128	31.72	0.930	0.156	225	17.4	59	31.49	0.929	0.156	217	15.5	56
	LoD 5	31.38	0.922	0.172	649	20.6	195	31.08	0.920	0.181	649	19.0	151	31.54	0.927	0.162	175	13.5	69	31.27	0.925	0.165	170	12.1	64
	LoD 4	31.09	0.918	0.183	446	14.9	230	30.92	0.920	0.188	446	13.7	167	31.23	0.922	0.174	136	10.6	79	30.94	0.919	0.178	133	9.5	72
	LoD																								